Electrochemical CO_2-to-ethylene conversion on polyamine-incorporated Cu electrodes

Xinyi Chen,[1,2,†] Junfeng Chen,[1,†] Nawal M. Alghoraibi,[1] Danielle A. Henckel,[1,3] Ruixian Zhang,[1] Uzoma O. Nwabara,[2,3] Kenneth E. Madsen,[1] Paul J. A. Kenis,[2,3] Steven C. Zimmerman,[1] and Andrew A. Gewirth[1,2,*]

[1]Department of Chemistry, University of Illinois at Urbana-Champaign, Urbana, IL, USA. [2]International Institute for Carbon Neutral Energy Research (WPI-I2CNER), Kyushu University, Fukuoka, JP. [3]Department of Chemical & Biomolecular Engineering, University of Illinois at Urbana-Champaign, Urbana, IL, USA. [†]These authors contributed equally to this work: Xinyi Chen, Junfeng Chen. *e-mail: agewirth@illinois.edu

Abstract

Electrochemical conversion of CO_2 into value-added chemicals holds promise to enable the transition to carbon neutrality. Enhancing selectivity toward a specific hydrocarbon product is challenging, however, due to numerous possible reaction pathways of CO_2 electroreduction. Here we present a copper-polyamine hybrid catalyst, developed through co-electroplating, that significantly increases the selectivity for ethylene production. The Faradaic efficiency for ethylene production is 87% ± 3% at -0.47 V versus reversible hydrogen electrode, with a full-cell energetic efficiency reaching 50% ± 2%. Raman measurements indicate that the polyamine entrained on the Cu electrode results in higher surface pH, higher CO content, and more stabilized intermediates relative to entrainment of additives containing little or no amine functionality. More broadly, this work shows that polymer incorporation can alter surface reactivity and lead to enhanced product selectivity at high current densities.

Introduction

Electrochemical CO_2 conversion to fuels offers an alternative pathway to produce carbon chemicals, which are traditionally produced by using carbon-intensive fossil fuels[1]. By utilizing the electricity generated from clean renewable energy sources, such as solar, wind, and geothermal energy, the CO_2 reduction reaction (CO2RR) additionally provides a way to store excess renewable electricity as chemical energy[2,3]. CO_2 reduction may also be utilized in direct atmospheric remediation schemes[4].

The pioneering work by Hori in the 1990s showed that Cu-based electrodes are the most efficient catalysts to reduce CO_2 to hydrocarbons[5,6], an insight that remains valid today. Intensive efforts have been directed toward enhancing CO2RR selectivity for one specific product[7,8]. The conversion of CO_2 to C_2 products (ethylene and ethanol) has been reported with enhanced selectivity on the Cu-based electrodes[9-18]. For example, the Faradaic Efficiency (FE) for ethylene production reached 60% on Cu nanocubes[9,10]. Alloying Cu with other metals also favors the production of ethylene (~60% FE)[11-13] or ethanol (~40% FE)[14,15]. Additionally, the

use of small molecules as additives to decorate the Cu electrodes is found to benefit the CO2RR to C_2 products[16,17]. The use of a flow-cell design for CO2RR not only enhances the reaction rate, it also enhances the formation of C_2 products on Cu by suppressing the hydrogen evolution reaction (HER)[19,20]. However, the FE for ethylene production remains ≤ 70% and the full-cell energetic efficiency (EE) for ethylene production remains ≤ 30%. Achieving high selectivity for ethylene production (FE > 80%) with low energy input (cell potential < 2.2 V) remains a major challenge in this field.

One way to increase CO2RR activity is through incorporation of an additive that could change intermediate stability on the electrode surface[17]. Unfortunately, small molecules added to the Cu electrode surface typically desorb and tend to leave in the flow cell[21]. Decoration of the electrode surface with a self-assembled monolayer (SAM) constructed by using a thiol or phosphonate also yields an unstable platform that quickly dissociates in the highly reducing and strong alkaline environment attendant the flow cell[22]. On the contrary, a polymer can be co-deposited with the Cu and remain entrained on the electrode surface with desired functionality[23,24]. As a related example, Cu deposits have been constructed in dendrimers featuring amine functionality[25]. We wondered how the incorporation of a functional polymer with a Cu electrode could affect CO2RR activity.

In this paper, we report the development of a Cu-polyamine catalyst for CO2RR – prepared using a co-electroplating scheme – which features exceptionally high FE and EE, particularly in the production of C_2 products. Polymer co-deposition with Cu has been examined for CO2RR previously[24], but these catalysts have not yet achieved high current density conversion. In this work, in 1 M KOH, the FE for ethylene production reached 72% (90% FE for C_2 products) at -0.97 V versus reversible hydrogen electrode (RHE; all potentials are with respect to this reference) with a partial ethylene current density of 312 mA/cm^2. By switching the electrolyte from 1 M KOH to 10 M KOH, the FE for ethylene production increased to 87% at a cathode potential of -0.47 V (93% FE for C_2 products), with the full-cell EE for ethylene production was 50% at a cell potential of 2.02 V. In situ Raman measurements revealed that a higher surface

pH, higher CO content, and more stabilized intermediates were observed on the Cu-polyamine electrode relative to Cu alone or Cu entrained with no amine polymer additives during CO2RR. The Raman results portray a catalyst in which stabilization of intermediates and a high surface pH improve the CO2RR selectivity to ethylene production.

Results

Synthesis and characterization of electrodes. To understand how polymer incorporation on the electrode might tune electrocatalysis activity, we prepared a group of polymers (P**i**, **i** = **1**-**5**) expected to display different local environments. The poly-*N*-(6-aminohexyl)acrylamide (P**1**) was synthesized by post-functionalizing poly(pentafluorophenyl acrylate)$_{100}$ (PPFPA$_{100}$, degree of polymerization = 100, polydispersity index = 1.05) using *N*-Boc-1,6-hexanediamine, followed by trifluoro acetic acid (TFA) deprotection (Supplementary Note 1). The resulting amino polymer P**1** was purified by dialyzing against water and characterized by using nuclear magnetic resonance (NMR, Supplementary Figs. 1-2). Methylated polymers P**2**, P**3**, and P**4** were prepared by methylating P**1** with different amounts of MeI (Supplementary Note 2). The degree of methylation was determined by using quantitative ^{1}H NMR (Supplementary Fig. 3). During the methylation process, methyl groups replaced hydrogen atoms on the amines randomly and resulted in a mixture of R-NHMe, R-NMe$_2$, and R-NMe$_3^+$ groups. The product that contains only trimethyl ammonium was defined as the 100% methylated polymer. P**2** was found to have 35% methylation and P**3** exhibited 65% methylation. P**4** was 100% methylated. P**5**, which has a different side chain length relative to P**1**, was prepared following the same procedure used for P**1** synthesis (Supplementary Note 3).

Following the synthesis of polymer P**i**, the copper-polymer (Cu-P**i**) electrode was prepared by co-electrodeposition. Each electrode was comprised of a carbon fiber paper-based gas diffusion layer (GDL) substrate on which the catalyst was electrodeposited. As shown in Fig. 1a, the Cu-P**i** electrode was prepared in a plating bath containing 3 mM $CuSO_4$, 12 μM P**i**, 0.1 M Na_2SO_4, and 0.5 M H_2SO_4. A pure Cu electrode (Cu alone) was prepared in the same plating

bath without polymer addition. Supplementary Figs. 5-6 show the wettability of all the samples on a GDL. The contact angle for the Cu alone electrode was found to be ca. 120º whereas the contact angle for the Cu-P**i** (**i**=**1**-**5**) electrode was ca. 145º. Thus, the addition of P**i** (**i**=**1**-**5**) makes the electrode more hydrophobic.

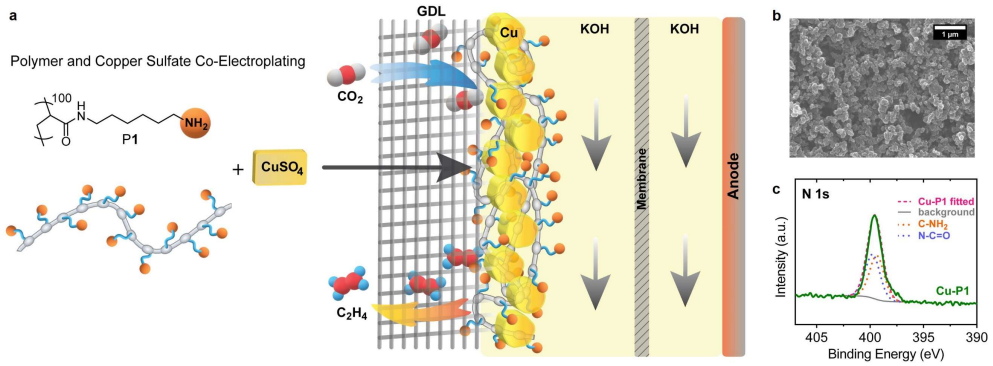

Fig. 1 | Preparation of the Cu-polymer catalyst. a, Schematic illustration of P**1** and Cu co-electroplating on the GDL. **b**, SEM image of the Cu-P**1** electrode. **c**, N 1s XPS spectrum of the Cu-P**1** electrode.

The Cu-P**i** electrode was characterized by using scanning electron microscopy (SEM). Fig. 1b and Supplementary Fig. 7a-c show the SEM images obtained from Cu-P**i** electrodes. All of the Cu-P**i** samples exhibit an agglomerated series of particles (identified as Cu by using EDX) that adopt spherical shapes with diameters between 100-200 nm. Thus, the electrodeposition of Cu with different P**i** does not substantially change the catalyst morphology. Supplementary Fig. 8 shows a cross-sectional SEM obtained from Cu-P**1** on a GDL. In addition to the fibrous GDL, Supplementary Fig. 8 shows a smooth layer (right) associated with the presence of Cu and a rougher discontinuous layer (left) associated with the backside of the GDL. XRD obtained from the different electrodes was identical (Supplementary Fig. 9).

Fig. 1c shows the N 1s photoemission spectrum of Cu-P**1**, which exhibits a peak at ca. 400 eV. This XPS component was fit to include both amine and amide groups, with corresponding peaks at 399.4 eV and 399.7 eV, respectively[26]. Thus, P**1** is retained on the electrode surface. Supplementary Fig. 10 shows the N 1s XPS spectra from Cu-P**2**, Cu-P**3**, and Cu-P**4**. The XPS shows the presence of a new peak at 402 eV, which is associated with trimethyl ammonium (R-NMe_3^+)[27]. The intensity of the ammonium peak was found to increase from Cu-P**2** to Cu-P**4**,

which is consistent with the increasing degree of methylation. Cu XPS (Supplementary Fig. 11) reveals the presence of Cu_2O and Cu on the electrodes.

Electrochemical CO_2 conversion. To evaluate the catalytic performance for the CO2RR, the Cu-P**i** electrode was utilized in a flow reactor described previously, where both CO_2 gas and KOH electrolyte were continuously introduced to the cell[19]. Fig. 2 shows the FEs for all products obtained during CO2RR using each Cu-P**i** electrode in 1 M KOH.

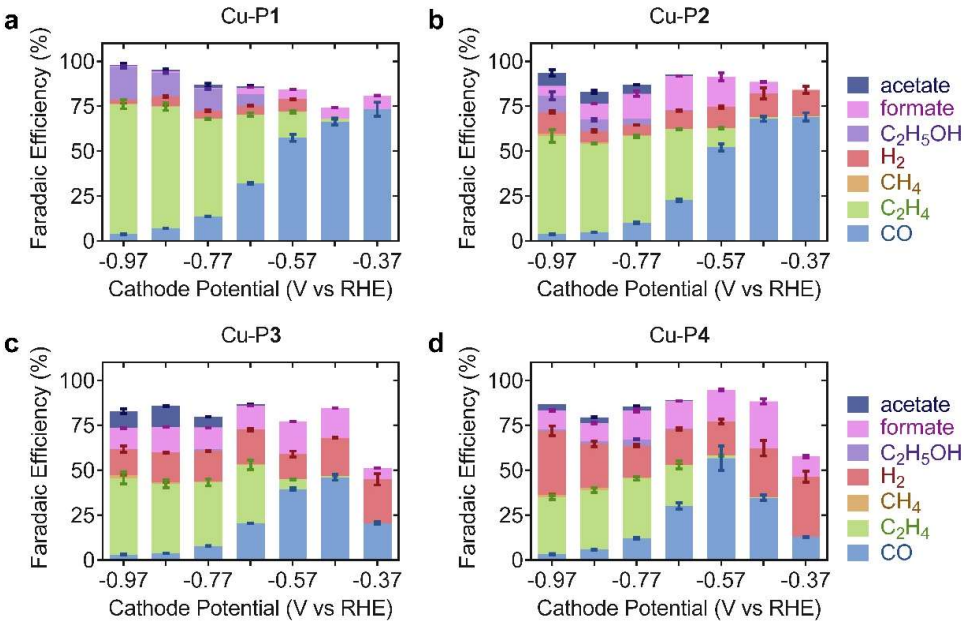

Fig. 2 | Electrochemical CO_2 conversion on the Cu-Pi electrodes. Faradaic efficiencies for all products on **a**, Cu-P**1**, **b**, Cu-P**2**, **c**, Cu-P**3**, and **d**, Cu-P**4** in 1 M KOH electrolyte.

For Cu-P**1**, the production of CO started at -0.27 V and reached a maximum FE of 73% at a cathode potential of -0.37 V. CO was found to be the dominant product at relatively low overpotentials (from -0.37 V to -0.57 V). As the cathode potential was made more negative, the FE for CO production decreased while the FEs for both ethylene and ethanol production increased. This trend is consistent with the assumption that the adsorbed CO is an intermediate for the formation of C_2 products, as has been suggested previously[28,29]. At -0.97 V, the FE for C_2 product formation on Cu-P**1** reached 90% (72% FE for ethylene production + 18% FE for ethanol production) with a total current density of 433 mA/cm^2 in 1 M KOH. By comparison,

the FE for ethylene production from the Cu alone electrode was only 27% at a current density of 207 mA/cm^2 under the same conditions and at the same potential (Supplementary Figs. 12-13). Thus, the addition of P**1** to the electrode leads to a FE increase of 45% for ethylene production. H_2 evolution was suppressed on Cu-P**1**, with the FE for H_2 evolution lower than 7% throughout the potential range examined, likely due to the higher surface pH for this catalyst relative to the others (*vide infra*). Consequently, the Cu-P**1** electrode exhibits excellent selectivity for the electroreduction of CO_2 to C_2 products. Supplementary Figs. 14-15show that no CO_2 reduction products were obtained using Ar in place of CO_2. Reduction of $^{13}CO_2$ yielded only ^{13}C labeled ethylene, further ruling out the possibility of polymer degradation to ethylene (Supplementary Fig. 16). Supplementary Fig. 17 shows that P**1** physiosorbed to the Cu electrode exhibits substantially less reduction current relative to Cu-P**1**. Supplementary Fig. 18 shows that the mono-amine mimic **2** (Supplementary Note 4) co-deposited with Cu is quickly deactivated during CO2RR. Finally, Supplementary Fig. 19 shows Cu-P**5** exhibits a decreased FE for ethylene production at more negative cathode potentials.

The Cu-P**4** electrode exhibits different CO2RR activity relative to that from Cu-P**1**. H_2 was found to be one of the main products on the Cu-P**4** electrode. The FE for H_2 production was 20-35% at all applied potentials. We note that high FE for H_2 production is typically favored on the carbon-based electrodes[30]. The production of formate was also favored on Cu-P**4** compared to that on Cu-P**1**. The high FEs for both hydrogen and formate production on Cu-P**4** lead to a low FE for C_2 product formation. At -0.97 V, the FEs for ethylene and ethanol production only reached 32% and 1% on the Cu-P**4** electrode, respectively.

For Cu-P**2** and Cu-P**3**, which exhibit reduced degree of methylation relative to Cu-P**4**, the selectivity for electroreduction of CO_2 to ethylene is greater than that in Cu-P**4**. At a cathode potential of -0.97 V, the FE for ethylene production on the Cu-P**2** and Cu-P**3** electrodes was 55% and 43%, respectively. In addition, the H_2 evolution was suppressed on Cu-P**2** and Cu-P**3** compared to that on Cu-P**4** likely due to the lower level of methylation.

Supplementary Fig. 13 shows the potential-dependent current density for CO_2 reduction on

each Cu-P**i** electrode in 1 M KOH. At less negative potentials (-0.27 V to -0.57 V), the four Cu-P**i** electrodes exhibited similar current densities for the CO2RR. As the potential became more negative (-0.67 V to -0.97 V), the current density was found to decrease in the order from Cu-P**1** to Cu-P**4**. At -0.97 V, the current density on Cu-P**1**, Cu-P**2**, Cu-P**3**, and Cu-P**4** was 433 mA/cm^2, 348 mA/cm^2, 305 mA/cm^2, and 232 mA/cm^2, respectively.

Overall, there is a strong correlation between the degree of methylation on each Cu-P**i** electrode and their CO2RR activity. The FE for ethylene production increases with higher hydrogen contents in the polymers: Cu-P**4** < Cu-P**3** < Cu-P**2** < Cu-P**1** whereas the FE for H_2 evolution increases with higher degree of methylation: Cu-P**1** < Cu-P**2** < Cu-P**3** < Cu-P**4**. Thus, the pendant amino groups in P**1** are likely the key factor promoting ethylene formation during CO_2 reduction while methyl groups favor H_2 evolution. One possibility for the better performance on Cu-P**1** is that the presence of H atoms in the amino groups at or near the electrode surface could act to change the reactivity (i.e., facilitate H transfer or interact with the CO2RR intermediates) or even surface pH. In addition, amines are known to react and bind CO_2 molecules[31,32]. Thus, amino groups in P**1** may help the electrode with CO_2 capture, leading to a higher local concentration of CO_2 or carbonate molecules on the electrode surface.

In situ electrochemical Raman spectroscopy measurements. To further understand how amino groups in P**1** promotes the CO2RR, in situ Surface-Enhanced Raman Spectroscopy (SERS) was performed during CO2RR in a cell described previously[13]. Fig. 3 shows the SERS spectra obtained from Cu-P**1**, Cu-P**4**, and Cu alone during the CO2RR. At open circuit potential (OCP), all three electrodes exhibit 3 peaks at 417 cm^{-1}, 515 cm^{-1}, and 620 cm^{-1} in the lower energy region. These three peaks are associated with the presence of Cu_2O[33,34]. In the higher energy region, the electrodes additionally exhibit two peaks at 1067 cm^{-1} and 1324 cm^{-1} at OCP, which correspond to carbonate and bicarbonate, respectively[35]. The water band at 1600 cm^{-1} was also observed on all three electrodes at OCP.

At a cathode potential of -0.47 V, the spectrum collected from Cu-P**1** exhibits several new peaks. In particular, there are new peaks at 293 cm^{-1} and 351 cm^{-1}. These two peaks are

177 associated with the frustrated ρ(Cu-C-O) rotational mode and the ν(Cu-CO) stretching mode,
178 respectively[36,37]. By comparison, the SERS spectra obtained from Cu-P**4** and Cu alone shows
179 little evidence for the Cu-CO binding in the same energy region. Thus, the Cu-P**1** electrode
180 exhibits higher CO content on the electrode surface during the CO2RR relative to the Cu-P**4**
181 and Cu alone electrodes. This increased CO concentration may facilitate C-C coupling and
182 ethylene production. Supplementary Table 1 shows the ratio of CO to Cu_2O – previously used
183 as a marker for increased ethylene production[13] – is substantially enhanced for the Cu-P**1**
184 catalyst.

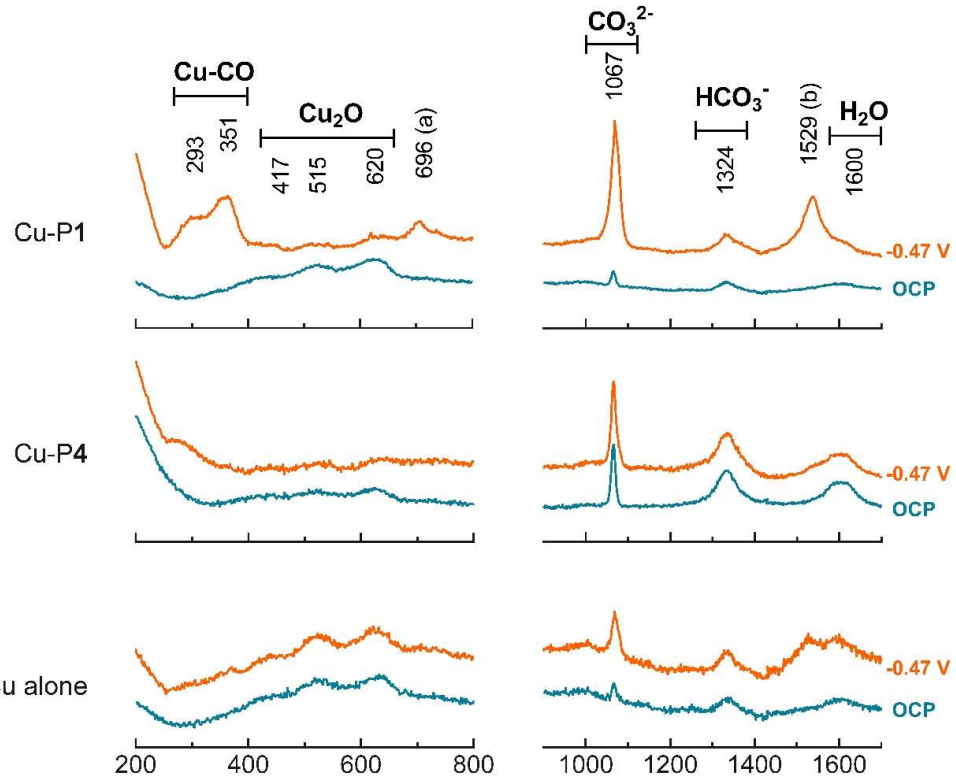

Fig. 3 | In situ electrochemical Raman spectroscopy measurements during CO2RR. SERS spectra obtained from Cu-P**1**, Cu-P**4**, and Cu alone at OCP (blue) and a cathode potential of -0.47 V (orange).

185 In addition to peaks related to Cu-CO binding, the Cu-P**1** electrode also exhibits two other
186 new peaks at 696 cm^{-1} (peak a) and 1529 cm^{-1} (peak b) at -0.47 V. The assignments for these
187 two peaks are under debate. In a recent study, peaks a and b were assigned to the adsorbed

188 carboxylate anion $*CO_2^-$ by DFT calculations and ^{13}C isotopic shift experiments[38]. Operando
189 Fourier transform infrared spectroscopy (FTIR) measurements also revealed peaks related to
190 CO2RR intermediates[39]. In particular, a peak at 1559 cm^{-1} was assigned to the asymmetric
191 stretching bond of $*CO_2^-$. The higher intensity of peak b on the Cu-P**1** electrode relative to the
192 Cu alone electrode shows that intermediates are stabilized on Cu-P**1**. The stabilization of
193 intermediates on Cu-P**1** might be the origin of the enhanced CO2RR activity. Peaks a and b
194 could not be observed on the Cu-P**4** electrode, consistent with the somewhat poorer CO2RR
195 activity on Cu-P**4**.

196 The relative ratio of carbonate to bicarbonate peaks in the SERS spectra provides a measure
197 of the surface pH[40]. Fig. 3 and Supplementary Fig. 20 show that the peak area ratio of
198 carbonate/bicarbonate on the three electrodes is different, indicating a different surface pH at
199 each electrode during the CO2RR. Supplementary Fig. 21shows the calibration curve for the
200 surface pH calculation from the carbonate and bicarbonate peaks and the calculated surface pH
201 values on each electrode are listed in Supplementary Table 2. Fig. 4 shows the surface pH
202 change on different electrodes at OCP and -0.47 V. At OCP, the Cu alone electrode exhibits a
203 surface pH of 9.5. This pH value is lower than that expected for 1 M KOH alone, because CO_2
204 reacts quickly with OH^- to form bicarbonate. The bicarbonate reacts further to form carbonate.
205 Thus, the reaction between CO_2 and OH^- near the electrode surface leads to a lower surface pH
206 relative to that of the bulk electrolyte. The Cu-P**1** electrode exhibits a surface pH value of 9.7
207 at OCP which is higher than that found for the Cu alone electrode. The origin of this increase
208 likely relates to the presence of amino groups at the electrode surface. A protonated organic
209 amino group typically exhibits a pK_a between 10-11, comparable with the pK_a for bicarbonate
210 (pK_a = 10.3). Therefore, an acid-base equilibrium exists on the Cu-P**1** electrode surface as
211 follows:

212 $$HCO_3^- + R-NH_2 \leftrightarrow CO_3^{2-} + R-NH_3^+ \quad (1)$$

213 The presence of amine shifts the equation to the right resulting in increased amounts of CO_3^{2-}
214 and consequently higher surface pH values. Cu-P**4** also exhibits a relatively high surface pH of

9.8. In this case the pH increase relative to the Cu alone electrode likely relates to OH^- ion attraction to the polycationic structure ($R\text{-}NMe_3^+$)[41,42].

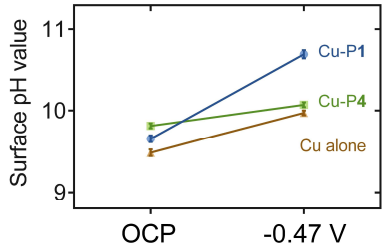

Fig. 4 | Calculated surface pH on different electrodes.

At a cathode potential of -0.47 V, the surface pH values of all three electrodes are found to increase compared to those at OCP. The Cu-P**1** electrode exhibits the highest surface pH value of 10.7, whereas the Cu-P**4** and Cu alone electrodes both exhibit pH values around 10.0-10.1 at this potential. Supplementary Fig. 22 reports SERS spectra obtained from Cu-P**5** in 1 M KOH. An increase in surface pH of 0.4 unit from 9.3 to 9.7 was found on Cu-P**5**. These pH values are substantially higher than those used in prior work[24] with polymer-modified Cu electrodes. The origin of the increased pH for the Cu-P**1** electrode likely relates to the presence of protonated amines on the electrode surface. Indeed, a previous report suggests that $R\text{-}NH_3^+$ donates a proton to a carbamate intermediate, making $R\text{-}NH_2$ during the CO2RR in a capture and reaction cycle[31]. The increased amount of $R\text{-}NH_2$ and decreased amount of $R\text{-}NH_3^+$ shift Equation (1) further to the right, leading to increased [CO_3^{2-}] and thus an increased pH. In addition, the proton functionality of P**1** could be serving as a surface proton relay, allowing for a faster deprotonation rate of HCO_3^- on Cu-P**1** compared to Cu-P**4**. The higher surface pH on the Cu-P**1** electrode might be the origin of the enhanced CO_2 reduction activity relative to other electrodes[10,43-46].

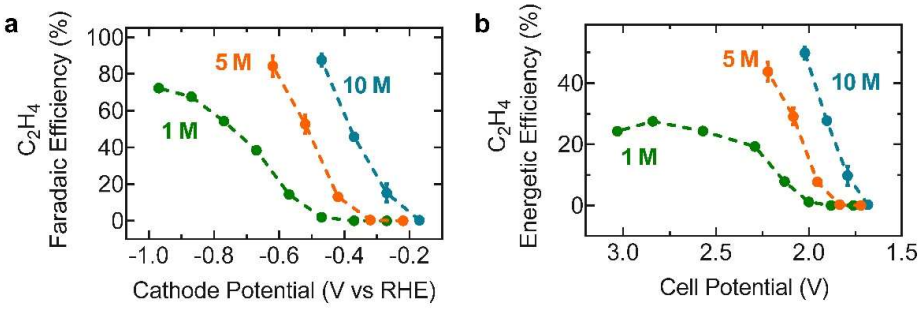

Fig. 5 | Electrochemical characterization of the Cu-P1 catalyst in different concentrations of KOH electrolyte. a, Faradaic efficiency for C_2H_4 production as a function of cathode potential. **b**, Energetic efficiency for C_2H_4 production as a function of cell potential.

Investigating CO2RR activity in alkaline media. The use of an alkaline electrolyte is believed to favor the production of ethylene, by lowering the energy barrier of CO_2 activation, facilitating C-C coupling, and suppressing H_2 evolution[10,43-46]. To investigate the beneficial role of pH, the CO2RR was performed using a series of more concentrated KOH electrolytes. The FEs for ethylene production on Cu-P**1** in 1 M, 5 M or 10 M KOH are plotted in Fig. 5a as a function of cathode potential. The figure shows the FE for ethylene production increases with higher concentrations of KOH. In 1 M KOH, the onset of ethylene production occurred at a cathode potential of -0.47 V and the FE for ethylene production on Cu-P**1** reached a maximum value of 72% at -0.97 V.

In 10 M KOH, ethylene production initiated at −0.17 V, which is the same potential where CO production started on this electrode (Supplementary Figs. 23-24). Additionally, the onset potential for ethylene production is shifted positively by 300 mV relative to that in 1 M KOH. The FE for ethylene production reaches 87% at a cathode potential of -0.47 V in 10 M KOH. To our knowledge, this value is the highest reported (Supplementary Table 3). The electroreduction of CO_2 to ethylene in 5 M KOH electrolyte was also found to have a higher FE and smaller overpotential compared to that in 1 M KOH. Ethylene evolution commenced at -0.32 V in 5 M KOH and the FE reached 84% at -0.62 V. Overall, the selectivity for ethylene production is strongly correlated to [KOH][10,43]. The better catalytic performance in 10 M KOH

is believed to result from the lower activation barriers for C-C coupling from activated CO on the Cu electrode surface[40-43]. We note that the use of highly concentrated alkaline electrolytes might result in an overestimation of the FEs for gas products due to CO_2 consumption in the electrolyte[47]. In this work, the FE difference (ca. 12-15%) among the different electrolytes is larger than the putative overestimation error, indicating selectivity enhancement by switching to more concentrated alkaline electrolyte actually occurs. Additionally, the positive shift of the onset potential for CO_2-to-ethylene conversion in more concentrated KOH electrolyte reveals better CO2RR activity. In the future, a two-step reduction with an initial CO_2-to-CO conversion and a following CO-to-ethylene conversion will be helpful to prevent CO_2 consumption by the electrolyte.

The use of a more concentrated electrolyte also reduces the overpotential at the anode (Supplementary Table 4). This reduction in overpotential leads to a higher energy efficiency. The EE of ethylene production on Cu-P**1** is plotted against cell potential in Fig. 5b. The figure clearly shows that the EE for ethylene production increases with higher electrolyte concentration: 1 M KOH < 5 M KOH < 10 M KOH. The full-cell EE achieved 50% at a cell potential of 2.02 V in 10 M KOH with the half-cell EE reaching 72%. (Half-cell EE was calculated by assuming the overpotential of oxygen evolution reaction is zero.) This EE at both the full-cell and half-cell level is, to our knowledge, higher than any results reported previously (Supplementary Table 3). We note the use of high concentration electrolytes may raise cost and pose durability issues; issues that may be diminished by using a membrane electrode assembly in place of the flow cell used here[48-50].

In situ Raman was performed on Cu-P**1** in 10 M KOH at a potential of -0.47 V where maximum ethylene production occurs. Supplementary Fig. 25 shows the Raman spectra obtained in 10 M KOH and Supplementary Fig. 26 reports the corresponding pH values. In this case, as well, an increase in pH relative to bare Cu is observed from 10.2 at OCP to 11.1 at -0.47 V. The higher surface pH value in 10 M KOH than that in 1 M KOH may be one of the reasons for the better catalytic performance.

The persistence of P**1** at the negative potentials attendant CO2RR was measured by using postmortem N XPS. Supplementary Fig. 27 shows the N 1s XPS spectrum collected from Cu-P**1** following 3 h of use for the CO2RR. The normalized intensity of the N 1s XPS peak (with respect to C 1s) before and after CO2RR was 38% and 34%, respectively, indicating that P**1** was retained during the electroreduction process. Supplementary Figs. 28-29 show that the SEM and XRD of the different electrodes after CO2RR was similar to that obtained prior to CO2RR. Similarly, GC analysis obtained using Ar in place of CO_2 shows no evidence for N-containing products (Supplementary Fig. 14). Thus, P**1** was relatively unchanged during the CO2RR.

Supplementary Fig. 30 shows the results of a test of Cu-P**1** stability in 1 M KOH at a cathode potential of -0.77 V. After 3 h use, the FE for ethylene production starts to decrease while the FE for H_2 evolution begins to increase. This behavior is similar to that seen when using Cu alone in a GDL and likely relates to corrosion in this configuration[10,43]. Prior work shows the GDL loses hydrophobicity during electrocatalysis, which leads to performance loss[51,52]. Using a PTFE-based electrode instead of one based on carbon might improve stability[43]. Improving the stability of Cu-based electrodes on a GDL or other substrates is presently a focus of research worldwide.

Conclusion

In this work, we decorated Cu electrodes with a stable amine-containing additive exhibiting different degrees of methylation. The Cu-P**1** electrode, which presents amino groups, exhibits the best CO2RR activity towards ethylene production at high current density and selectivity. The origin of this behavior is the higher CO content and higher surface pH on Cu-P**1** relative to the other electrodes. The higher surface pH is a consequence of the presence of the amine. The presence of P**1** may also help to stabilize intermediates during the CO2RR.

Overall, this work presents a strategy to enhance electrochemical CO_2-to-ethylene conversion through the introduction of a polymer that is entrained on the electrode surface.

These findings provide a method by which designer CO2RR catalysts for high rate conversion may be constructed.

Methods

Catalysts preparation. All Cu samples are comprised of a carbon fiber paper-based gas diffusion layer (GDL) substrate (Sigracet 35 BC, Ion Power Inc.) on which a catalyst was electrodeposited. The plating baths for Cu-P**i** (**i** =**1**-**4**) and Cu alone were made from 3 mM $CuSO_4$, 0.1 M Na_2SO_4, and 0.5 M H_2SO_4, with or without the addition of 12 μM P**i**. All chemicals were obtained from Sigma-Aldrich. Galvanostatic electrodeposition on the GDL at a constant current density of -4 mA/cm^2 was performed until a final deposition charge of 2 C/cm^2 was reached to generate samples with identical loading. The back side of GDL substrate was fixed to a micro glass slide with a double-sided tape, giving one-sided deposition of Cu. Pt wire was used as the counter electrode. A "leakless" Ag/AgCl (eDAQ) electrode was used as the reference electrode. Before electrodeposition, the GDL was pretreated by sputtering 10 nm of Cu using an AJA Orion-8 Magnetron Sputtering System. The thickness of the Cu deposit was ca. 2 μm as determined by profilometry. Electroactive surface areas for the different electrodes were similar (Supplementary Table 5).

Materials Characterization. Scanning electron microscopy (SEM) images were obtained utilizing a JEOL 7000F Analytical SEM. X-ray photoelectron spectroscopy (XPS) was performed with a Physical Electronic PHI 5400 instrument. X-Ray diffraction (XRD) patterns were obtained by using a Bruker D8 Advance X-ray Diffractometer. Contact angle measurements were conducted using a Ramé-Hart contact angle goniometer (Model 250). Gas chromatography–mass spectrometry (GC-MS) spectra were obtained by using a Waters GCT Premier EI. NMR spectroscopy was recorded using a Carver Bruker 500 NMR spectrometer in the NMR Laboratory, School of Chemical Science, University of Illinois. NMR spectra were processed by using MestReNova (v12.0.3). The chemical shift (δ) is listed in ppm and the coupling constants (J) are in Hz.

CO_2 Electroreduction in a Flow Reactor. Electroreduction experiments and product analysis were conducted in a flow reactor setup described previously[19,53]. A syringe pump (PHD 2000, Harvard Apparatus) was used to pump electrolyte at a constant flow rate of 0.2 or 0.5 mL min^{-1} over the cathode

GDL. A mass flow controller (Smart Trak 2, Sierra Instruments) was used to flow CO_2 gas (S.J. Smith Welding Supply) at a flow rate of 7 standard cubic centimeters per minute (SCCM) behind the cathode GDL. The CO_2 electroreduction activity for all catalysts was measured by holding a constant cathode potential with respect to a Ag/AgCl electrode (3 mol kg^{-1} KCl, RE-5B, BASi) using an Autolab PGSTAT-30, EcoChemie potentiostat. All cathode potentials were converted to the reversible hydrogen electrode (RHE) by using the Nernst equation: E (vs. RHE) = E (vs. Ag/AgCl) + 0.209 V + 0.0591 V × pH. A GDL with an IrO_2 loading of 1 mg/cm^2 was used as the counter electrode[53]. Anode potentials were recorded by a multimeter (AMPROBE 15XP-B) with respect to a Ag/AgCl electrode.

Three minutes after the potential was applied, the gaseous product stream was sampled automatically and diverted for analysis in a gas chromatograph (Thermo Finnigan Trace GC) equipped with both a thermal conductivity detector (TCD) and a flame ionization detector (FID). The exit electrolyte containing liquid products was collected and analyzed in a Carver B500 NMR spectrometer using a ^1H NMR technique described previously[19]. Dimethyl sulfoxide (DMSO) was used as an internal standard.

In situ electrochemical Raman measurements. In situ Raman measurements were carried out by utilizing a spectro-electrochemical flow cell described previously[13]. A 2.0 mm thick polyether ether ketone (PEEK) spacer with a 0.5 × 2 cm hole was placed between a quartz window and the cathode GDL. A syringe pump (PHD 2000, Harvard Apparatus) was used to pump 1 M KOH at a constant flow rate of 1.0 mL min^{-1} over the GDL through the PEEK spacer. CO_2 gas was introduced to the back of the GDL in a stainless-steel chamber at a flow rate of 7 SCCM controlled by a mass flow controller (Smart Trak 2, Sierra Instruments). For each in situ Raman measurement, the Raman spectrum was accumulated by 180 single acquisitions, with an exposure time of 1 second each. Working electrodes were formed from Cu-P**i** or Cu alone electrodeposited on a GDL. Cathode potentials were applied in the potentiostatic mode with respect to a Ag/AgCl reference electrode (3 mol kg^{-1} KCl, RE-5B, BASi) and reported with respect to RHE. To be consistent with the electrolysis measurements, Raman spectra were obtained 3 minutes after the potential was initially applied. Pt wire was used as the counter electrode.

Data availability

The data that support the results and other findings of this study are available from the corresponding authors upon reasonable request.

References

1 Nitopi, S. *et al.* Progress and Perspectives of Electrochemical CO_2 Reduction on Copper in Aqueous Electrolyte. *Chem. Rev.* **119,** 7610−7672 (2019).

2 Verma, S., Lu, S. & Kenis, P. J. A. Co-electrolysis of CO_2 and glycerol as a pathway to carbon chemicals with improved technoeconomics due to low electricity consumption. *Nat. Energy* **4,** 466-474 (2019).

3 Montoya, J. H. *et al.* Materials for solar fuels and chemicals. *Nat. Mater.* **16,** 70-81 (2016).

4 Hepburn, C. *et al.* The technological and economic prospects for CO_2 utilization and removal. *Nature* **575,** 87-97 (2019).

5 Hori, Y., Kikuchi, K., Murata, A. & Suzuki, S. Production of Methane and Ethylene in Electrochemical Reduction of Carbon Dioxide at Copper Electrode in Aqueous Hydrogencarbonate Solution. *Chem. Lett.* **15,** 897-898 (1986).

6 Hori, Y., Wakebe, H., Tsukamoto, T. & Koga, O. Electrocatalytic Process of CO Selectivity in Electrochemical Reduction of CO_2 at Metal Electrodes in Aqueous Media. *Electrochim. Acta.* **39,** 1833-1839 (1994).

7 Luc, W. *et al.* SO_2-Induced Selectivity Change in CO_2 Electroreduction. *J. Am. Chem. Soc.* **141,** 9902-9909 (2019).

8 Zhang, H. *et al.* Computational and experimental demonstrations of one-pot tandem catalysis for electrochemical carbon dioxide reduction to methane. *Nat. Commun.* **10,** 3340 (2019).

9 Yin, Z. *et al.* Cu_3N Nanocubes for Selective Electrochemical Reduction of CO_2 to Ethylene. *Nano Lett.* **19,** 8658-8663 (2019).

10 Wang, Y. *et al.* Copper Nanocubes for CO_2 Reduction in Gas Diffusion Electrodes. *Nano Lett* **19,** 8461-8468 (2019).

11 Hoang, T. T. H. *et al.* Nanoporous Copper-Silver Alloys by Additive-Controlled Electrodeposition for the Selective Electroreduction of CO_2 to Ethylene and Ethanol. *J. Am. Chem. Soc.* **140,** 5791-5797 (2018).

12 Ma, S. *et al.* Electroreduction of Carbon Dioxide to Hydrocarbons Using Bimetallic Cu-Pd Catalysts with Different Mixing Patterns. *J. Am. Chem. Soc.* **139,** 47-50 (2017).

13 Chen, X. *et al.* Controlling Speciation during CO_2 Reduction on Cu-Alloy Electrodes. *ACS Catal.* **10,** 672-682 (2019).

14 Li, Y. C. *et al.* Binding Site Diversity Promotes CO_2 Electroreduction to Ethanol. *J. Am. Chem. Soc.* **141,** 8584-8591 (2019).

15 Morales-Guio, C. G. *et al.* Improved CO_2 reduction activity towards C_{2+} alcohols on a tandem gold on copper electrocatalyst. *Nat. Catal.* **1,** 764-771 (2018).

16 Hoang, T. T. H. *et al.* Nanoporous Copper Films by Additive-Controlled Electrodeposition: CO_2 Reduction Catalysis. *ACS Catal.* **7,** 3313-3321 (2017).

17 Li, F. *et al.* Molecular tuning of CO_2-to-ethylene conversion. *Nature* **577,** 509-513 (2020).

18 Wang, Y. *et al.* Catalyst synthesis under CO_2 electroreduction favours faceting and promotes renewable fuels electrosynthesis. *Nat. Catal.* **3,** 98-106 (2019).

19 Ma, S. *et al.* One-Step Electrosynthesis of Ethylene and Ethanol from CO_2 in an Alkaline Electrolyzer. *J. Power Sources* **301,** 219-228 (2016).

20 Weekes, D. M. *et al.* Electrolytic CO_2 Reduction in a Flow Cell. *Acc. Chem. Res.* **51,** 910-918 (2018).

21 Schmitt, K. G. & Gewirth, A. A. In Situ Surface-Enhanced Raman Spectroscopy of the Electrochemical Reduction of Carbon Dioxide on Silver with 3,5-Diamino-1,2,4-Triazole. *J. Phys. Chem. C* **118,** 17567-17576 (2014).

22 Widrig, C. A., Chung, C. & Porter, M. D. The electrochemical desorption of n-alkanethiol monolayers from polycrystalline Au and Ag electrodes. *J. Electroanal. Chem.* **310,** 335-359 (1991).

23 Tsakova, V. *et al.* Electrochemical incorporation of copper in polyaniline layers. *Electrochimica. Acta.* **46,** 4213-4222 (2001).

24 Ahn, S. *et al.* Poly-Amide Modified Copper Foam Electrodes for Enhanced Electrochemical Reduction of Carbon Dioxide. *ACS Catal.* **8,** 4132-4142 (2018).

25 Mingqi, Z., Li, S. & M., C. R. Preparation of Cu Nanoclusters within Dendrimer Templates. *J. Am. Chem. Soc.* **120,** 4877-4878 (1998).

26 Mohtasebi, A. *et al.* Interfacial Charge Transfer between Phenyl-Capped Aniline Tetramer Films and Iron Oxide Surfaces. *J. Phys. Chem. C* **120,** 29248-29263 (2016).

27 Sylvestre, J.-P. *et al.* Surface Chemistry of Gold Nanoparticles Produced by Laser Ablation in Aqueous Media. *J. Phys. Chem. B* **108,** 16864-16869 (2004).

28 Schouten, K. J. P. *et al.* A New Mechanism for the Selectivity to C_1 and C_2 Species in the Electrochemical Reduction of Carbon Dioxide on Copper Electrodes. *Chem. Sci.* **2,** 1902-1909 (2011).
29 Kortlever, R. *et al.* Catalysts and Reaction Pathways for the Electrochemical Reduction of Carbon Dioxide. *J. Phys. Chem. Lett.* **6,** 4073-4082 (2015).
30 Jiang, H. *et al.* Defect-rich and ultrathin N doped carbon nanosheets as advanced trifunctional metal-free electrocatalysts for the ORR, OER and HER. *Energy Environ. Sci.* **12,** 322-333 (2019).
31 Khurram, A. *et al.* Promoting Amine-Activated Electrochemical CO_2 Conversion with Alkali Salts. *J. Phys. Chem. C* **123,** 18222-18231 (2019).
32 Kortunov, P. V., Siskin, M., Paccagnini, M. & Thomann, H. CO_2 Reaction Mechanisms with Hindered Alkanolamines: Control and Promotion of Reaction Pathways. *Energy & Fuels* (2016).
33 Deng, Y. *et al.* In Situ Raman Spectroscopy of Copper and Copper Oxide Surfaces during Electrochemical Oxygen Evolution Reaction: Identification of Cu^{III} Oxides as Catalytically Active Species. *ACS Catal.* **6,** 2473-2481 (2016).
34 Jiang, S., Klingan, K., Pasquini, C. & Dau, H. New Aspects of Operando Raman Spectroscopy Applied to Electrochemical CO_2 Reduction on Cu Foams. *J. Chem. Phys.* **150,** 041718 (2019).
35 Frantz, J. D. Raman spectra of potassium carbonate and bicarbonate aqueous fluids at elevated temperatures and pressures: comparison with theoretical simulations. *Chem. Geol.* **152,** 211–225 (1998).
36 Akemann, W. & Otto, A. The effect of atomic scale surface disorder on bonding and activation of adsorbates: vibrational properties of CO and CO_2 on copper. *Surf. Sci.* **287,** 104-109 (1993).
37 Gunathunge, C. M. *et al.* Spectroscopic Observation of Reversible Surface Reconstruction of Copper Electrodes under CO_2 Reduction. *J. Phys. Chem. C* **121,** 12337-12344 (2017).
38 Chernyshova, I. V., Somasundaran, P. & Ponnurangam, S. On the origin of the elusive first intermediate of CO_2 electroreduction. *Proc. Natl. Acad. Sci.* **115,** E9261-E9270 (2018).
39 Firet, N. J. & Smith, W. A. Probing the Reaction Mechanism of CO_2 Electroreduction over Ag Films via Operando Infrared Spectroscopy. *ACS Catal.* **7,** 606-612 (2016).
40 Davis, A. R. & Oliver, B. G. A Vibrational-Spectroscopic Study of the Species Present in the CO_2-H_2O System. *J. Solution Chem.* **1,** 329-339 (1972).
41 Klitzing, R. & Moehwald, H. Proton Concentration Profile in Ultrathin Polyelectrolyte Films. *Langmuir* **11,** 3554-3559 (1995).
42 Zhang, Y., Tsitkov, S. & Hess, H. Proximity does not contribute to activity enhancement in the glucose oxidase-horseradish peroxidase cascade. *Nat Commun* **7,** 13982 (2016).
43 Dinh, C.-T. *et al.* CO_2 electroreduction to ethylene via hydroxide-mediated copper catalysis at an abrupt interface. *Science* **360,** 783–787 (2018).
44 Varela, A. S., Kroschel, M., Reier, T. & Strasser, P. Controlling the selectivity of CO_2 electroreduction on copper: The effect of the electrolyte concentration and the importance of the local pH. *Catal. Today* **260,** 8-13 (2016).
45 Schouten, K. J. P., Pérez Gallent, E. & Koper, M. T. M. The influence of pH on the reduction of CO and CO_2 to hydrocarbons on copper electrodes. *J. Electroanal. Chem.* **716,** 53-57 (2014).
46 Raciti, D., Mao, M., Park, J. H. & Wang, C. Local pH Effect in the CO_2 Reduction Reaction on High-Surface-Area Copper Electrocatalysts. *J. Electrochem. Soc.* **165,** F799-F804 (2018).
47 Ma, M. *et al.* Insights into the carbon balance for CO_2 electroreduction on Cu using gas diffusion electrode reactor designs. *Energy Environ. Sci.* **13,** 977-985 (2020).
48 Xia, C. *et al.* Continuous production of pure liquid fuel solutions via electrocatalytic CO_2 reduction using solid-electrolyte devices. *Nat. Energy* **4,** 776-785 (2019).
49 Lee, J. *et al.* Electrochemical CO_2 reduction using alkaline membrane electrode assembly on various metal electrodes. *J. CO_2 Util.* **31,** 244-250 (2019).
50 Gabardo, C. M. *et al.* Continuous Carbon Dioxide Electroreduction to Concentrated Multi-carbon Products Using a Membrane Electrode Assembly. *Joule* **3,** 2777-2791 (2019).
51 Tomas, M. *et al.* Modification of gas diffusion layers properties to improve water management. *Mater. Renew. Sustain. Energy* **6** (2017).
52 Yu, S. *et al.* Study on hydrophobicity loss of the gas diffusion layer in PEMFCs by electrochemical oxidation. *RSC Adv.* **4,** 3852-3856 (2014).
53 Verma, S. *et al.* The Effect of Electrolyte Composition on the Electroreduction of CO_2 to CO on Ag based Gas Diffusion Electrodes. *Phys. Chem. Chem. Phys.* **18,** 7075-7084 (2016).

Acknowledgements

The authors gratefully acknowledge the support of the International Institute for Carbon Neutral Energy

Research (WPI-I2CNER), sponsored by the Japanese Ministry of Education, Culture, Sports, Science and Technology. D.A.H., U.O.N., and P.J.A.K. gratefully acknowledge Shell's New Energy Research and Technology (NERT) program for providing funding. J.C. and S.C.Z. acknowledge support of the National Science Foundation (NSF CHE-1709718). We thank Mass Spectrometry Lab (especially Dr. Furong Sun and Dr. Xiuli Mao) for performing GC/MS measurements. We thank Dr. Richard T. Haasch for performing XPS and the SCS machine shop for their help in designing the in situ flow cell for the SERS measurements. We also thank SCS NMR lab for their help in NMR measurements.

Author contributions

X.C. and N.M.A. prepared the Cu-**Pi** electrodes and performed the electrochemistry experiments. J.C. synthesized the polymers and performed NMR experiments. X.C. conducted the SEM and XRD experiments. X.C. and D.A.H. carried out the Raman measurements. R.Z. analyzed the XPS data. U.O.N. prepared the anode electrodes. K.E.M. did the contact angle measurements. A.A.G., S.C.Z., and P.J.A.K. conceived the project and supervised the research work. X.C., J.C., and A.A.G. wrote the manuscript with input from the other authors.

Competing interests

The authors declare no competing financial interests.

Additional information

Supplementary information is available for this paper at https://doi.org/

Reprints and permissions information is available at www.nature.com/reprints.

Correspondence and requests for materials should be addressed to A.A.G.

Publisher's note: Springer Nature remains neutral with regard to jurisdictional claims in published maps and institutional affiliations.